Proceedings of the INMM & ESARDA Joint Virtual Annual Meeting
August 23-26 & August 30-September 1, 2021

Nuclear materials location based on Neutron time-of-flight and Fast Coincidence Counting

Clement DEYGLUN

Institute for Radiological Protection and Nuclear Safety (IRSN), Fontenay-Aux-Roses, France

Abstract

Reprocessing, nuclear fuel fabrication, or uranium enrichment require large facilities that contain many glovebox, tanks and pipes where uranium and/or plutonium can build up. During the cleaning and dismantling of these facilities, the quantity of fissile materials need to be evaluated for nuclear material accounting and control, criticality safety, radiation protection and waste management. Holdup measurements are usually performed using gamma-ray techniques or neutron measurements with He-3 detectors. During these measurements, many factors can influence the result, such as the geometry of the container, the presence of uncharacterized shields and matrix, the location of the source, its distribution and isotopic composition, etc. Neutron time-of-flight event detection and fast coincidence counting can be used to discriminate neutron from gamma and establish the location of nuclear materials. MCNPX-PoliMi is used to model plutonium in a glovebox and a tank. An array of plastic scintillators is simulated around the inspected object and a post-processing macro based on ROOT simulates the response of the acquisition system (energy threshold, energy resolution, time jitter, etc.). The neutron time-of-flight technique is performed to identify fission signatures and source location. Afterwards, plutonium mass could be evaluated.

Keywords: holdup, plutonium, neutron, time-of-flight, simulation

1. Introduction

Reprocessing, fuel fabrication, or enrichment require large facilities that contain many gloveboxes, tanks and pipes where plutonium can build up. The goal in measuring holdup is to quantify the amount of nuclear material in equipment to ensure all nuclear materials are accounted for. Holdup measurement is essential to verify nuclear material inventories in nuclear process facilities, but also for safeguards, and criticality safety.

Two measurement technics are mainly used for holdup measurement: gamma-ray spectrometry based on the Generalized Geometry Holdup method (GGH), using NaI scintillator, or HPGe detector [1, 2, 3] and neutron coincidence counting (with large polyethylene-moderated ^{3}He slab detectors) [2, 3, 4, 5, 6]. Measuring the nuclear materials deposit in such cases challenges the capabilities and compromises the accuracy of gamma techniques because of very large attenuation effects by equipment and deposits, and the necessary assumptions to describe the deposits (point, line, area, or volume). Neutrons are highly penetrating and less affected by mechanisms such as self-absorption and, therefore, applicable to measure large deposits contained in massive equipment. Nevertheless, they are difficult to protect from the background and a description of the source distribution is still necessary.

The paper presents the study of a system based on neutron time-of-flight event detection and fast coincidence counting for plutonium holdup measurement without any assumption on the source localization or distribution.

2. Measurement Theory

2.1. The spontaneous fission process

Fission is a fast process and fragments de-excitation takes place at early stage after scission through successive emission of neutrons and gamma-rays, namely the prompt fission neutrons and the prompts fission gamma-rays. In this paper, prompts fission neutrons and gamma-rays are considered simultaneously emitted. The number of emitted prompt fission neutrons or gamma-rays, referred as multiplicity, is characterized by a statistical distribution. In average, 2.15 prompt neutrons and 6.99 prompt gamma-rays are emitted per spontaneous fission of ^{240}Pu. The speed of prompt fission neutrons depends on their energy (in MeV), which is driven by a Watt distribution [7]:

$$Proba(E_n) = c \times exp(-E/a)\, sinh\left(\sqrt{bE}\right) \quad (1)$$

With a = 0.799 and b = 4.903 for ^{240}Pu [7] (c is a normalization parameter) and the relation between neutron's energy and speed: $E_n = \frac{1}{2} m_n c^2 \frac{v^2}{c^2}$. The speed of prompt fission gamma-rays is about 30 cm/ns, whereas the speed of prompt fission neutrons is lower than 4 cm/ns. The speed difference between neutrons and gamma-rays is a key factor to discriminate these particles.

2.2. Principle

Figure 1 shows a schematic drawing of the system concept. The system considered consists of many plastic scintillators (slave detectors) and one NaI(Tl) scintillator (trigger detector) placed around the inspected object.

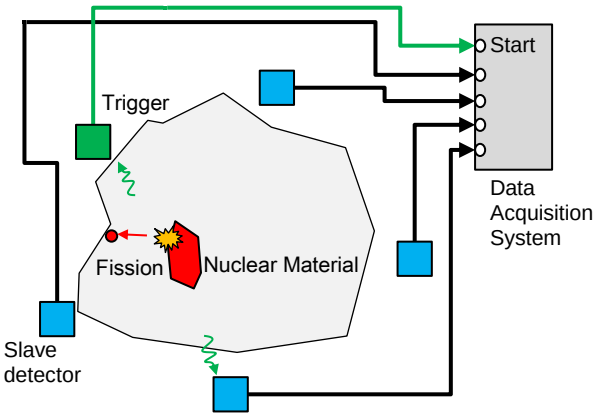

Figure 1. Schematic drawing of the system concept.

The slave detectors and the trigger detector are located around the inspected object. All the detectors are placed without any knowledge of the nuclear material localization or distribution. Δ_{gamma} nanoseconds after the fission of the nuclear material, if at least one gamma-ray reaches the trigger detector, then the acquisition by the slave detectors starts. The time of flight (TOF) between the detection in the trigger and the slave detectors is measured. If Δ_{gamma} is small enough, the TOF can be considered equal to the time between the fission and the detection of a prompt fission particle. The TOF measurement allows the discrimination between gamma-rays and neutrons.

In the case of a point source, for each "trigger-slave" pair (slave detector number *i*), the number of coincidences at the time of flight "tof", is driven by the following equation:

$$C^{i}{}_{gn}(tof) = Fiss \times \overline{\nu_{gn}} \times \left(Proba_{g}^{trig}\right) \times \left(Proba_{n}^{i}(tof)\right) \quad (2)$$

With

- $Fiss$ is the number of fissions ;
- $\overline{\nu_{gn}}$ is the average number of gamma-neutron pairs per fission ;
- $Proba_{g}^{trig}$ is the probability to detect a least one prompt gamma-ray by the trigger detector:
  $Proba_{g}^{trig} = Att_{g} \times \varepsilon^{trig}{}_{geo} \times \varepsilon^{trig}{}_{int}$ (3) ;
- $Proba_{n}^{i}(tof)$ is the probability to detect, within slave detector *i*, at least one prompt neutron "tof" nanoseconds after the trigger:
  $Proba_{n}^{i}(tof) = Att_{n} \times \varepsilon^{i}{}_{geo} \times \varepsilon^{i}{}_{int} \times Prob^{i}(tof)$ (4)

Where

- Att_{g} and Att_{n} are the attenuations of gamma-rays and neutrons before the detection ;
- $\varepsilon^{trig}{}_{geo}$ and $\varepsilon^{i}{}_{geo}$ are the geometric efficiencies of the detectors (trigger or slave number *i*) ;
- $\varepsilon^{trig}{}_{int}$ and $\varepsilon^{i}{}_{int}$ are the intrinsic detection efficiencies of the detectors (trigger or slave number *i*) ;
- $Prob^{i}(tof)$ is the probability to detect one neutron "tof" nanoseconds after the detection of an associated prompt gamma-ray. This probability depends on the energy distribution of the prompt fission neutrons described by the Watt spectra.

During the measurement, for each detected event, i.e. trigger detector activated plus at least one slave detector activated, two inputs are obtained: the TOF of the detected particle and the energy deposit inside the slave detector. Based on these information, the holdup measurement takes three steps:

1. The estimation of the source localization and distribution, from the meshing of the inspected object in voxels ;
2. The TOF-distributions deconvolution to estimate the number of fissions in each voxel ($Fiss_{vox}$) (cf. Equation 2) ;
3. The estimation of the source activity.

These three steps are described below.

2.3. Source Localization and Distribution

The first step of the measurement treatment is the source localization, described in the Figure 2. This method allows source(s) localization without any assumption on the source(s) distribution(s) or location(s). After the "localization & distribution" step, each voxel has a weight proportional to the probability of presence of the source.

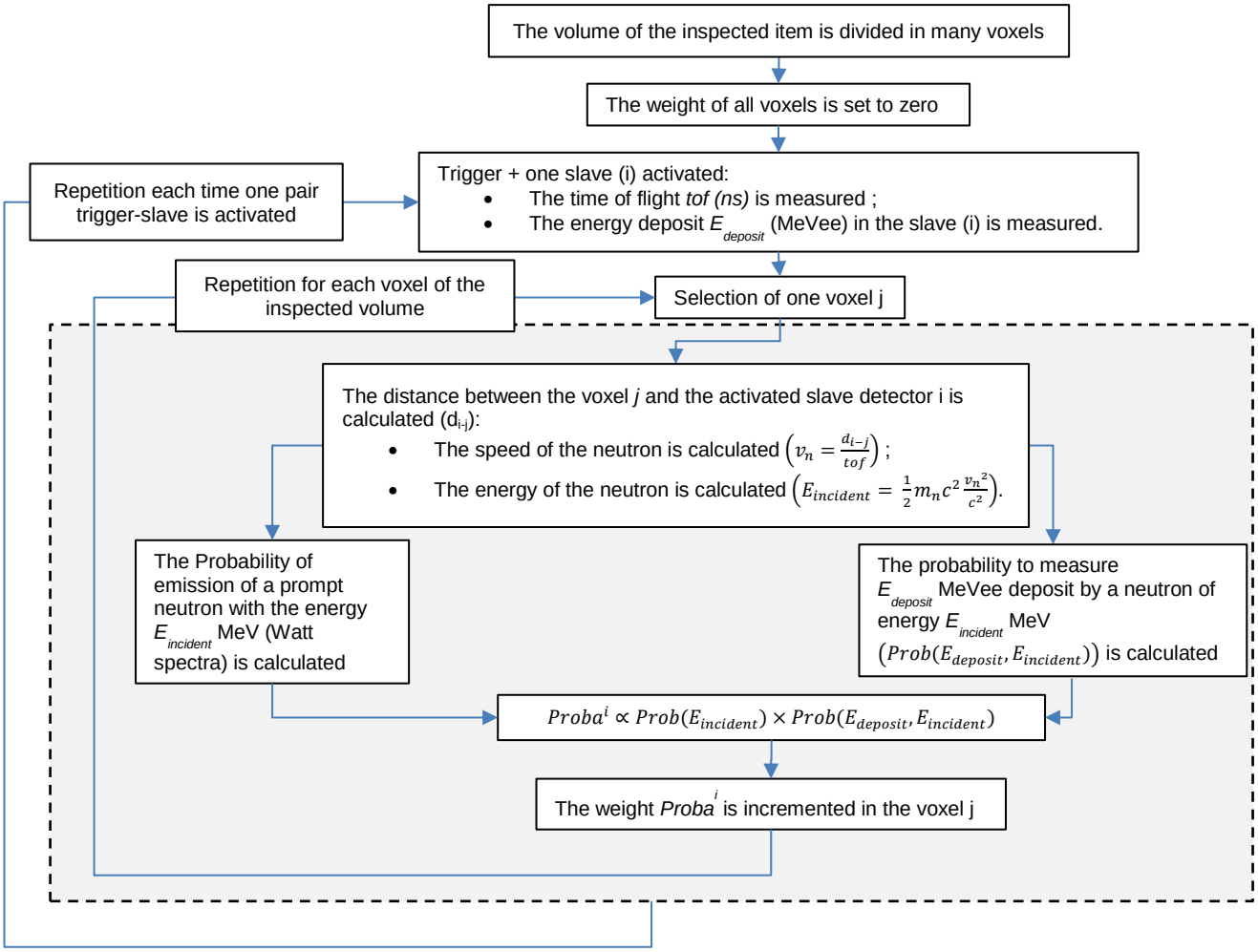

Figure 2. Source localization process.

2.4. TOF-distribution and deconvolution

Equation 2 is generalized to take into account the multiple localizations of the source in N voxels:

$$C^{i}{}_{gn}(tof) = \sum_{vox=0}^{N} Fiss_{vox} \times \overline{\nu_{gn}} \times Att_g \times Att_n \times \left(\varepsilon^{trig}{}_{geo} \times \varepsilon^{trig}{}_{int}\right) \times \left(\varepsilon^{i}{}_{geo} \times \varepsilon^{i}{}_{int} \times Prob^{i}(tof)\right) \quad (5)$$

Where $Fiss_{vox}$ is the number of fissions in the voxel *vox*.

Based on the presence probability of each voxel and the TOF distribution calculated for each "trigger-slave" pair, the coefficient $Fiss_{voxel}$ is estimated for each voxel using Khi2 minimization method between measured and calculated TOF distributions (cf. Equation 5). Materials which contain elements with high atomic number, such as lead glass, have poor capability to attenuate fast neutrons. Hence, in first approximation neutrons attenuation is neglected: $Att_n \approx 1$. But prompt gamma-rays attenuation cannot be neglected and the attenuation coefficient Att_g is estimated based on another technic (for example transmission measurement with a reference source, or simulation). Based on these approximations:

$$C^{i}{}_{gn}(tof) \approx \sum_{vox=0}^{N} Fiss_{vox} \times \overline{\nu_{gn}} \times \left(Att_g \times \varepsilon^{trig}{}_{geo} \times \varepsilon^{trig}{}_{int}\right) \times \left(\varepsilon^{i}{}_{geo} \times \varepsilon^{i}{}_{int} \times Prob^{i}(tof)\right) \quad (6)$$

The total number of fissions is estimated by $Fiss_{tot} \approx \sum_{Vox=1}^{N} Fiss_{vox}$, where N is the number of voxels where the source has been detected.

3. Simulation

MCNPX is a well-known Monte Carlo code used for the simulation of neutrons and photons transport in geometries involving numerous materials [7]. The PoliMi extension [8, 9] simulates fission events and particles interactions one by one. In addition, neutrons and photons fission multiplicity distributions are implemented, and neutronss interaction and photon production are made correlated. At each collision, information on neutron and gamma collisions is recorded. The code output consists in information about each collision within cells defined as detectors: the type of collision, the collision target, the energy deposited, the time and position of the interaction, etc. A first post-processing macro based on the ROOT analysis platform [10] models specific detector characteristics: it converts the energy deposit of each particles interaction in detectors (in MeV) in light output (in MeVee) [11, 12], smears the light output by the energy resolution, and applies an energy threshold and a time jitter. Once the output of a realistic system is obtained, a second post-processing macro, also based on ROOT, applies the steps described in the previous paragraphs for source localization and activity estimation.

3.1. Setups Description

Two inspected objects are simulated: a cylindrical tank (1 cm thickness of iron) and a glovebox (2.5 cm thickness of lead glass). These two objects are inspected by a system composed of 6 slaves detectors (plastic scintillators 20×20×10 cm^3) and 1 trigger detector (NaI(Tl) scintillator 20×20×10 cm^3). The seven detectors are distributed homogeneously around the inspected object. The setups are presented in Figure 3**Erreur ! Source du renvoi introuvable.**.

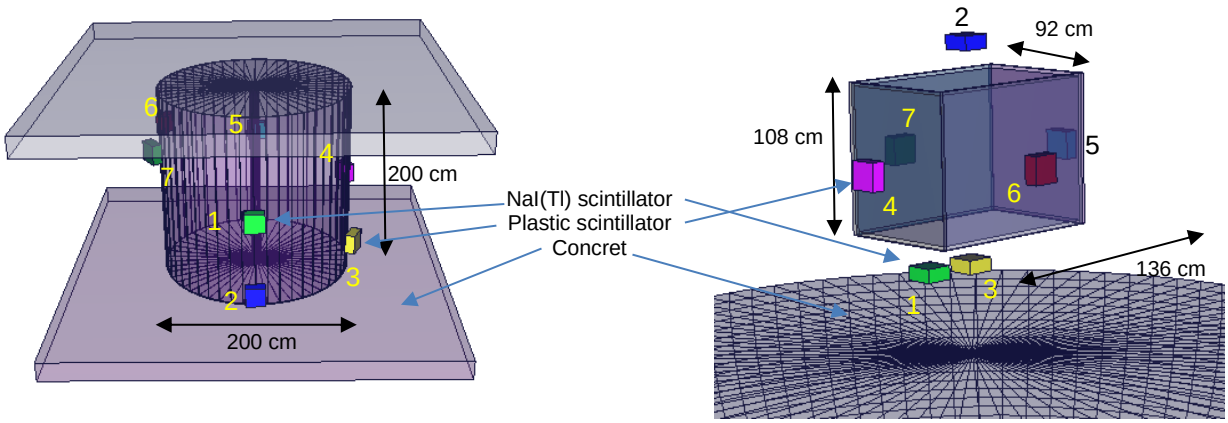

Figure 3. 3D view of detectors distribution around the inspected tank and glovebox.

Four ^{240}Pu source distributions are tested (Figure 4):

- Source 1 - Point source
- Source 2 - Linear source
- Source 3 - Surface source
- Source 4 - Volume source

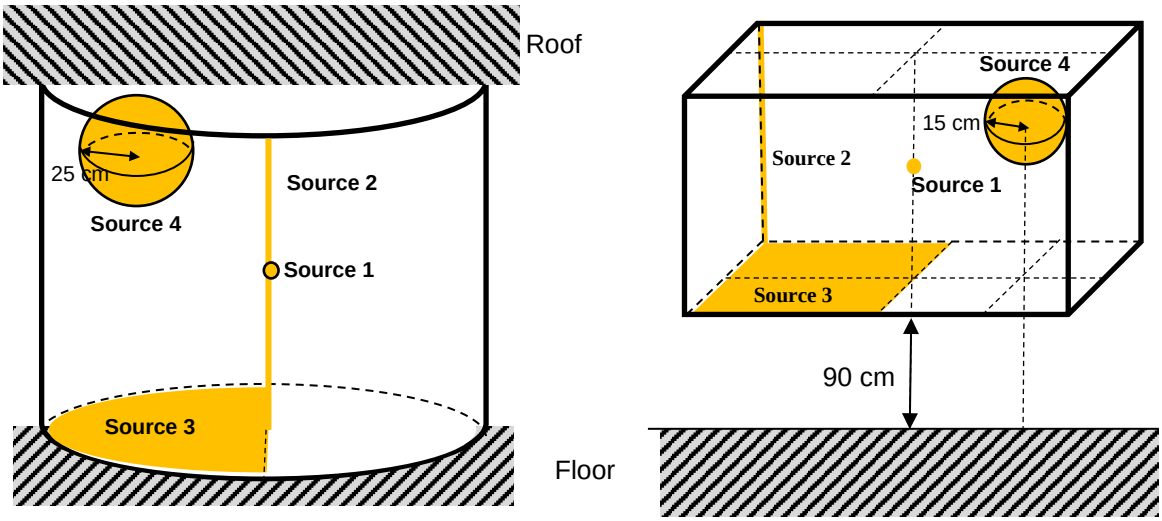

Figure 4. The four simulated sources distributions within the tank and the glovebox.

To simplify the simulation, many assumptions are made in the paper:

- Only spontaneous fissions of ^{240}Pu are considered ;
- No induced fissions are considered, neither (α-n) reactions nor β-decays ;
- The external background is not simulated.

3.2. Output

The setups presented in Figure 3 are simulated by MCNPX-PoliMi for the four ^{240}Pu sources distributions described in Figure 4. The code output is processed by a first ROOT macro to convert the simulated output to a realistic output. The TOF-distributions between detector n°1 (the trigger detector) and the slave detector n°2, resulting from this first post-processing are presented in Figure 5.

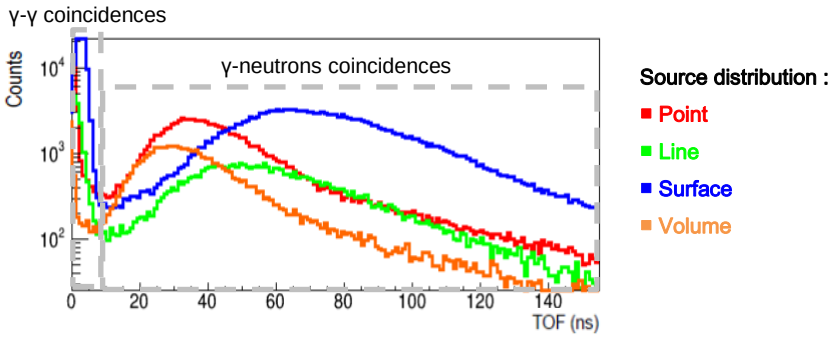

Figure 5. The TOF distributions for detectors 1-2, for the point source, line, surface and volume within the inspected glovebox.

The gamma-rays TOF is distributed between 0 ns and 10 ns, whereas neutrons TOF is distributed between 10 ns and 140 ns. The shape of the "neutron part" depends on the distance between the source and the detector, and the source distribution.

3.3. Localization of the source

Table 1 and Table 2 here after show the different results for the localization of the four simulated sources distributions. For each inspected object, the inspected volume is divided in 1040 voxels (20 min – 1 h calculation with an Intel Core Duo 2.00 GHz×2 computer) and 8840 voxels (2.5 h – 8 h calculation with an Intel Core Duo 2.00 GHz×2 computer). So two dimensions of voxel, close from detector's volume, are tested for each inspected object in the Table 1 and the Table 2.

Table 1. Source localization within the tank.

Source	Simulated localization	Calculated localization*	
		8840 voxels (Voxel's dimensions: 7.7×12.5×10.0 cm^3)	1040 voxels (Voxel's dimensions: 15.4×25.0×20.0 cm^3)
1 (point)	X = 0.0 cm Y = 0.0 cm Z = 100.0 cm	X = [- 15.3, 7.8] cm Y = [-17.4, 18.0] cm Z = [70.0, 140.0] cm	X = [-7.6, 7.8] cm Y = [-24.3, 24.3] cm Z = [60.0, 140.0] cm
2 (line)	X = [- 5.0, 5.0] cm Y = [- 5.0, 5.0] cm Z = [1.0, 190.0] cm	X = [-15.3, 7.8] cm Y = [-29.2, 18.0] cm Z = [50.0, 150.0] cm	X = [-23.0, 7.8] cm Y = [-24.3, 24.3] cm Z = [40.0, 160.0] cm
3 (surface)	X = [- 100.0, 0.0] cm Y = [- 100.0, 100.0] cm Z = 1.0 cm	X = [-53.8, -23.0] cm Y = [- 17.4, 41.6] cm Z = [0.0, 30.0] cm	X = [-53.8, - 23.0] cm Y = [-24.3, 49.3] cm Z = [0.0., 40.0] cm
4 (volume)	X = [- 75.0, 25.0] cm Y = [- 25.0, 25.0] cm Z = [145.0, 195.0] cm	X = [-84.6, -38.4] cm Y = [-41.0, 6.2] cm Z = [70.0, 190.0] cm	X = [- 84.6, -38.4] cm Y = [-49.3, 24.3] cm Z = [60.0, 200] cm

* Localization interval is calculated between the extremum of the voxels where the source is detected.

In the case of the inspected tank, source localization with "small" and "large" voxels are very close. The dimension of voxels has a little impact on the source localization, but the necessary time for calculation is 8 time higher with the small voxels than the large voxels.

Even if the source distribution is not perfectly calculated, the localization of the source is well estimated for the four sources. The dispersion of the source is correct in the XY plan, but not in Z axis: the Z-axis distribution of the point source and linear source appear very close. This bias is probably due to the impossibility to place detectors under and above the inspected tank.

Table 2. Source localization within the glovebox.

Source	Simulated localization	Calculated localization*	
		8840 voxels (Voxel's dimensions: 5×5×5 cm^3)	1040 voxels (Voxel's dimensions: 10×10×10 cm^3)
1 (point)	X = 0.0 cm Y = 0.0 cm Z = 140.0 cm	X = [-11.0, 14.0] cm Y = [-13.5, 11.5] cm Z = [132.5, 147.5] cm	X = [-6.0, 14.0] cm Y = [-13.5, 6.5] cm Z = [132.5, 152.5] cm
2 (line)	X = 65.5 cm Y = 43.0 cm Z = [92.0, 194.0] cm	X = [-66.0, -56.0] cm Y = [26.5, 41.5] cm Z = [137.5, 157.5] cm	X = [-66.0, -56.0] cm Y = [26.5, 36.5] cm Z = [132.5, 152.5] cm
3 (surface)	X = [- 66.0, 0.0] cm Y = [- 44.0, 44.0] cm Z = 93.0 cm	X = [-36.0, -16.0] cm Y = [-18.5, 16.5] cm Z = [92.5, 102.5] cm	X = [36.0, -6.0] cm Y = [-23.5, 16.5] cm Z = [92.5, 102.5] cm
4 (volume)	X = [25.0, 55.0] cm Y = [- 15.0, 15.0] cm Z = [145.0, 175.0] cm	X = [29.0, 54.0] cm Y = [-18.5, 16.5] cm Z = [147.5, 167.5] cm	X = [34.0, 54.0] cm Y = [-23.5, 16.5] cm Z = [152.5, 172.5] cm

* Localization interval is calculated between the extremum of the voxels where the source is detected.

As previously noted, source localization with "small" and "large" voxels are very close. The dimension of voxels has a little impact on the source localization, but impact dramatically the necessary time of calculation.

In the case of the inspected glovebox, the localization of the source is well estimated for the four sources. But as shown in Figure 6, the dispersion of the source is under-estimated if the real dispersion is too large (> 60 cm). Thanks to detectors under and above the glovebox, the Z-axis dispersion of the source is better estimated than in the inspected tank.

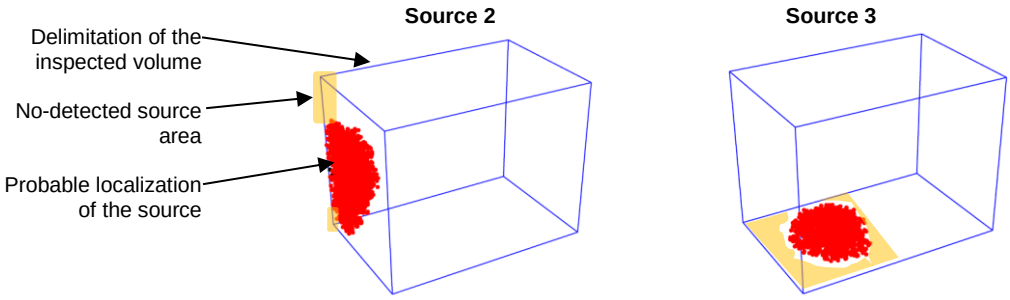

Figure 6. Under-estimation of the source 2 (line) and 3 (surface) dispersion (voxel's dimension: 5.0×5.0×5.0 cm^3) in the inspected glovebox.

3.4. TOF-distributions deconvolution

Based on the probable localization of the source(s), the coefficient $Fiss_{vox}$ in Equation 6 is estimated for each voxel by Khi2 minimization method between the calculated TOF-distributions (Equation 6) and the observable TOF-distributions.

The source distribution estimation is very important for a deconvolution distribution close to the measurement. Figure 7 is an example of the impact of a bad estimation of the vertical distribution (axis Z) of the surface source (source 3) on the deconvolution of TOF distributions.

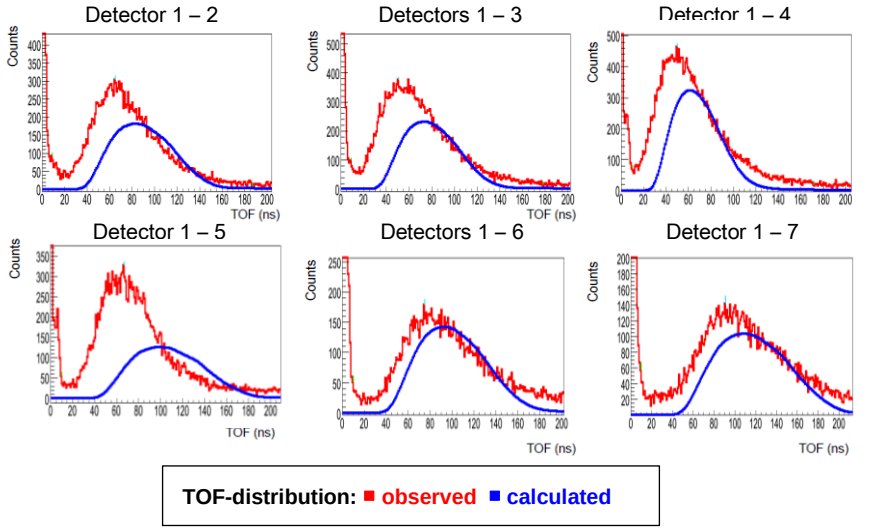

Figure 7. Comparison between the calculated TOF distributions (after deconvolution) and the observed TOF distributions for the source 3 within the inspected tank.

As previously noted, the estimation of the source localization and distribution is very important. It has a great impact on the TOF-distributions deconvolution, and so the number of fissions estimation.

3.5. Activity calculation

As shown in paragraph 3.4, error on the source distribution, but probably also the neglected attenuations of neutrons, have an impact on the TOF-distributions deconvolution and thus the estimation of the number of fissions. Such error is partially corrected using the total

number of measured coincidences trigger-slave detectors ($C_{gn}^{tot}(mesured)$) and calculated ($C_{gn}^{tot}(calculated)$) with Equation 6:

$$C_{gn}^{tot}(mesured) = C \times C_{gn}^{tot}(calculated) \quad (7)$$

Where C is the correction coefficient. After correction, the total number of fissions is estimated as follows:

$$Fiss_{total} \approx C \times \sum_{Vox=1}^{N} Fiss_{vox} \quad (8)$$

Based on Equation 8, Table 3 and Table 4 below show the estimation of the number of measured fissions.

Table 3. Number of fissions calculation within the tank.

Source	Number of simulated ^{240}Pu spontaneous fissions	Number of calculated fissions	
		8840 voxels (Voxel's dimensions: 7.7×12.5×10.0 cm^3)	1040 voxels (Voxel's dimensions: 15.4×25.0×20.0 cm^3)
1 (point)	2.00×10^9	5.32×10^9	5.02×10^9
2 (line)	2.00×10^9	4.36×10^9	6.40×10^9
3 (surface)	2.00×10^9	3.91×10^9	3.72×10^9
4 (volume)	2.00×10^9	4.97×10^9	4.89×10^9

Table 4. Number of fissions calculation within the glovebox.

Source	Number of simulated ^{240}Pu spontaneous fissions	Number of calculated fissions	
		8840 voxels (Voxel's dimensions: 5×5×5 cm^3)	1040 voxels (Voxel's dimensions: 10×10×10 cm^3)
1 (point)	2.00×10^9	2.59×10^9	4.15×10^9
2 (line)	2.00×10^9	2.74×10^9	2.45×10^9
3 (surface)	2.00×10^9	2.99×10^9	3.62×10^9
4 (volume)	2.00×10^9	2.94×10^9	3.64×10^9

For the inspected tank and glovebox, an over-estimation of the number of fissions is observed despite the applied correction. But the number of simulated and calculated fissions are of the same order of magnitude, which is a very encouraging result for such large inspected objects. In previous study [13], better results were obtained with smaller detectors and a trigger detector placed inside the glovebox. It suggests that a better estimation of the geometrical efficiency could improve the number of fissions calculation.

The tested dimensions of voxels have a little impact on the source localization, but an important impact on the number of calculated fissions. Even if splitting the inspected volume into "small" voxels means long calculation time, it is necessary to have the best number of fissions estimation.

4. Conclusions

The paper shows the interest of measuring holdup using the combination of neutron time of flight measurement and gamma-neutron coincidences measurement technics. It is possible to estimate the localization, the source distribution and the number of fissions without any prior knowledge. This study used simple assumptions. In next study, complex simulations will be performed to test the technic in realistic conditions:

- Simulation of multiple sources ;

- Simulation of additional beta and (α,n) sources ;
- Simulation of the accidental coincidences ;
- Simulation of the outside background simulation.

These additional considerations should make the holdup measurement more difficult, but in the same time many parameters shall be optimized:

- Detectors dimensions and shapes ;
- Detectors distribution ;
- Voxels dimensions ;
- Correction of the neutrons attenuation.

Moreover, additional studies are needed to optimize the algorithm developed to localize the source(s), and deconvoluate the TOF-distributions for the number of fissions calculation.

5. References

1. P. A. Russo, "Gamma-Ray Measurements of Holdup Plant-Wide: Application Guide for Portable, Generalized Approach," Los Alamos National Laboratory Report LA-14206, June 2005.
2. D. L. Haggard, L. W. Brackbush, "Determination of the Radioactive Material and Plutonium Holdup in Ducts and Piping in the 327 Building," Pacific Northwest Laboratory Report PNL-10787, 1995.
3. J. Chevillon, R. Oddou, H. Schoech, M. Vincent, "Measurement of the Plutonium Hold-Up in Glove Box before Dismantling," *WM2015* Conference, Phoenix, Arizona, USA, March 15-19, 2015.
4. H. Tanaka, H. Nakamura, T. Hosoma, "Design of geometrical detector arrangement for extensive holdup measurement," *Symposium on international safeguards: Verification and nuclear material security*, Vienna, Austria, 29 Oct - 2 Nov 2001.
5. D.H. Beddingfield, H.O. Menlove, "Distributed source term analysis, a new approach to nuclear material inventory verification," Nuclear Instruments and Methods in Physics Research A 485 (2002) 797–804.
6. H. Nakamura et al., "Development and Implementation of GloveBox Cleanout Assistance Tool (BCAT) to Detect the Presence of MOX by Computational Approach," *M&C 2017*, Jeju, Korea, April 16-20, 2017.
7. D. B. Pelowitz, "MCNPX User's Manual Version 2.7.0," Los Alamos National Laboratory LA-CP-11-00438, April. 2011.
8. E. Padovani, et al., "MCNPX-PoliMi User's Manual," Polytechnic of Milan, Italy and University of Michigan, Ann Arbor, MI, April 2012.
9. S. A. Pozzi, E. Padovani, and M. Marseguerra, "MCNP-PoliMi: A Monte Carlo Code for Correlation Measurements," Nuclear Instruments and Methods A, 513, pp. 550–558, 2003.
10. R. Brun, F. Rademakers, ROOT "An object oriented data analysis framework," Nucl. Instrum. Meth. A389, 81–86, 1997.
11. E. C. Miller, S. D. Clarke, M. Flaska, S. Prasad, S. A. Pozzi, and E. Padovani, "MCNPX-PoliMi Post-Processing Algorithm for Detector Response Simulations," Journal of Nuclear Materials Management, Volume XL, Number 2, 2012.
12. S. A. Pozzi, E. Padovani, M. Flaska, and S. Clarke, "MCNPX-PoliMi Matlab Post-Processing Code Ver 1.9," ORNL/TM-2007/33, 2007.
13. C. Deyglun, "Time-of-Flight technic for nuclear material localization using plastic scintillators", ANIMMA2021 Conference, Prague, 2021.